# RESERVOIR CHARACTERIZATION OF UNCONVENTIONAL GAS SHALE RESERVOIRS: EXAMPLE FROM THE BARNETT SHALE, TEXAS, U.S.A.

*by Prerna Singh[1], Roger Slatt[1], Gabriel Borges[1], Roderick Perez[1], Romina Portas[1], Kurt Marfurt[1], Michael Ammerman[2], and William Coffey[2].*

*1. University of Oklahoma, Norman, Oklahoma, 73019*

*2. Devon Energy Corp., Oklahoma City, Oklahoma, 73102*

**ABSTRACT—**A multidisciplinary study utilizing log, core and 3D seismic has resulted in developing a log- , core- and seismic-based stratigraphic framework for regional mapping of stratigraphic and petrophysical units of the Barnett Shale in part of the Fort Worth Basin of Texas. To date, we have applied this workflow to our initial study area covering approximately 550 square miles. Nine lithofacies have been identified from long Barnett Shale cores. Carbonate-rich intervals are indicative of shallower-water environments, while clay-rich intervals are more indicative of deeper, quieter-water environments of deposition. The lithofacies are arranged in a predictable vertical stacking pattern of parasequences, representing shallowing-upward or deepening-upward depositional environments. The parasequences are continuous and mappable over the study area. Stratigraphic intervals defined from well data have been correlated to three 3D seismic volumes, and mapped regionally. In general, the Barnett Shale in this area thickens toward the northeast, closer to its source, but there is some variability in thickness trends within specific stratigraphic intervals. The workflow that has been developed is being extended to other areas of the Fort Worth Basin Barnett Shale play.

## INTRODUCTION

Shales have been traditionally considered to be hydrocarbon source and/or seal rocks. As attention to unconventional hydrocarbon resources has blossomed in recent years, shales have become recognized as containing major gas resources. However, there are substantial differences between this unconventional reservoir type and the traditional and better understood sandstone and carbonate reservoirs. New ideas and methods of reservoir characterization are required to reduce uncertainty in measuring volumetrics, in drilling and stimulating a well, and in gaining efficient production. We address some of theses issues encountered with the Barnett Shale based upon sound, integrated geological, geophysical, and engineering analysis.

The Barnett Shale is currently the most active shale gas play in the U.S, having produced >2.6TCF in recent years (Durham, 2007). Success with this play has been instrumental in initiating active pursuits of other Mississippian and Devonian shales in North America to find possible Barnett-like plays.

The Barnett Shale was deposited by the inundation of the Texas peninsula by a Mississippian sea (Adams, 1957) adjacent to the southeastern part of the southern Oklahoma aulocogen (Henry, 1982). The Barnett Shale unconformably overlies the Ordovician-age Viola/Ellenburger Group. It is overlain by the Pennsylvanian-age Marble Falls Limestone. The Barnett Shale is thickest in the northeastern part of the Fort Worth basin where it is divided into the Upper and Lower Barnett by the intermediate Forestburg limestone formation. To the south, the Barnett Shale thins and remains undifferentiated as the Forestburg pinches out.

This unconventional shale reservoir has in the past been considered to be 'homogeneous, undifferentiated black shale'. Our studies, in addition to other recent studies in the area (Loucks et al. 2007, Hickey et al. 2007, Bowker, 2007), show that there is significant variation in the internal stratigraphy of the Barnett Shale. This variable lithologic nature underscores the need to better understand depositional conditions prevalent during deposition of these fine grained rocks. Our current integrated core, wireline log and seismic study addresses the sedimentology, internal geometry, and lateral and vertical, cyclical depositional patterns in the Newark East field and adjoining areas, Fort Worth Basin of Texas (Fig. 1). The workflow that we have developed is a model for analysis of the Barnett and other gas shales over a broader geographic area.

## GEOLOGY

Continuous, long cores of Barnett Shale have been studied from three wells (Fig.1) to understand the depositional environment, stacking pattern and to build a sequence stratigraphic framework. The Barnett Shale has been divided into nine lithofacies based on visual core description, extensive petrography and mineralogy integrated with wire-line log data. Lithofacies are described below along with their systematic stacking patterns. The format follows such that it first discusses muddy facies deposited for the most part under low energy conditions *viz. siliceous non-calcareous mudstone, siliceous calcareous mudstone* and *micritic/ limy mudstone*. The next three facies discussed represent relatively high energy facies *viz. bottom current calcareous laminae deposit, fossiliferous deposit* and *silty-shaly (wavy) interbedded mudstone*; next the two diagenetic facies are discussed viz: *concretions and dolomitic mudstone*, followed by *phosphatic lithofacies* which was deposited in both low energy and high energy environments.

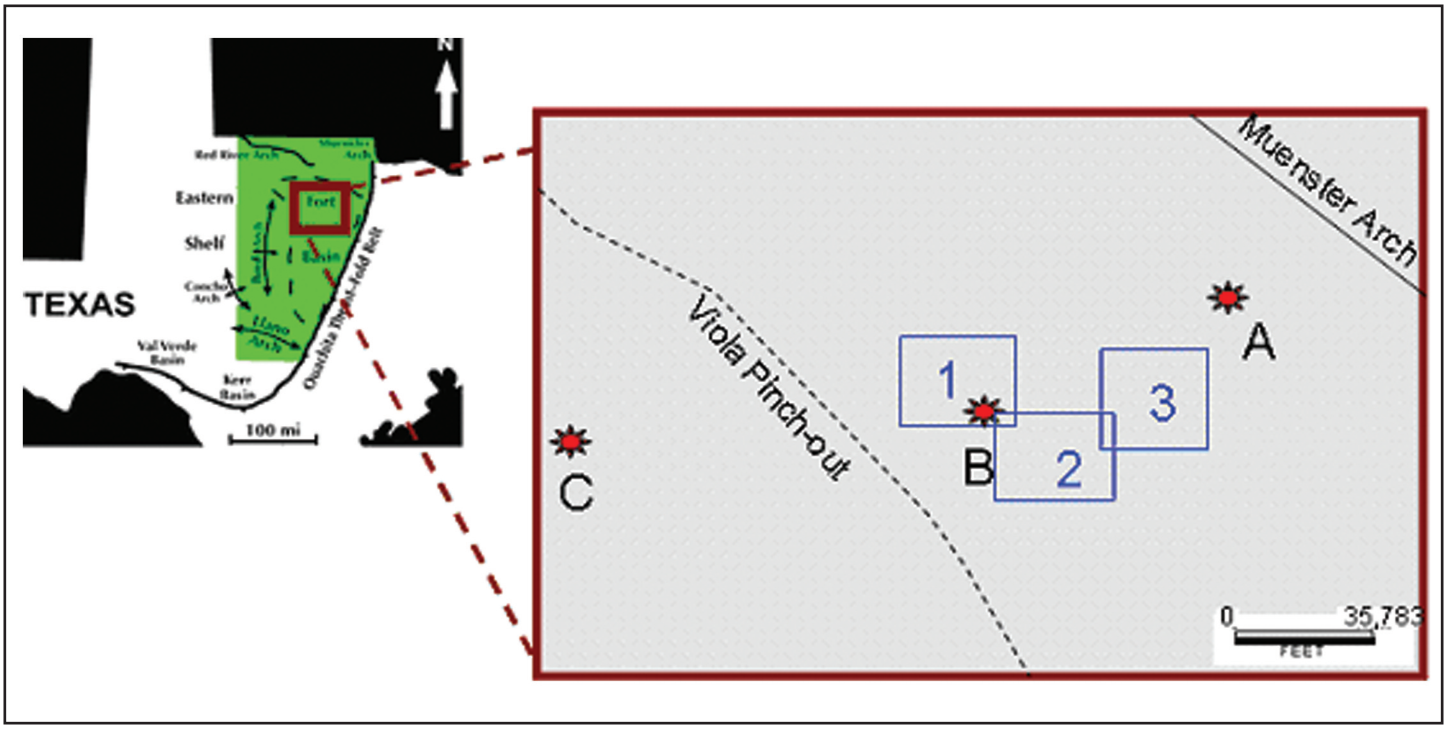


**Figure 1**. *Map showing the Fort Worth basin (Modified from Montgomery et al., 2005) and the location of the study wells A, B and C and the seismic survey areas 1, 2 and 3.*

***Siliceous Non-Calcareous Mudstone***

The *siliceous non-calcareous mudstone* facies is black, massive mudstone, which does not react with dilute hydrochloric acid. Petrography and mineralogic measurement indicates quartz and clays are the most dominant mineral components. Pyrite, phosphate peloids, calcite, dolomite, and ferroan dolomite are the minor components (Table 1).

The silica content is of both biogenic and detrital nature. Detrital quartz grains are of silt and finer sizes. Detrital quartz grains are often bound organically as agglutinated arenaceous forams (Papazis, 2005, Milliken et al. 2007) (Figure 2B). The common biogenic components are agglutinated forams and sponge spicules, which occur in variable abundance. The lack of any bioturbation and micro-sedimentary structures suggests a quiet water environment of deposition, dominated for the most part by suspension settling of the pelagic and hemipelagic sediments.

**Table 1**. *Mineralogy of the lithofacies*

| Facies Names | Silica including quartz and authigenic silica | | Clays | Calcite | | Dolomite (including Fe-dolomite) | | Mica | Phosphate | Glauconite | Pyrite |
|---|---|---|---|---|---|---|---|---|---|---|---|
| | *Average | Min-Max | | *Average | Min-Max | *Average | Min-Max | | | | |
| Siliceous Non –calcareous Mudstone | 30% | 20- >50% | 30-40% | 0-2% | 0-5% | 2-5% | 2-10% | 0-5% | 0-5% | - | 0-3% |
| Siliceous Calcareous mudstone | 25% | 15-30% | 30-40% | 10-15% | 5-40% | 2-5% | 2-15% | 0-5% | 0-5% | - | 0-3% |
| Bottom current Calcareous laminae deposit | *15% | | 20-25% | *35-40% | | *2-5% | | - | 0-5% | - | 5-7% |
| Concretion | *10-15% | | 20% | *55-60% | | - | | - | 1% | - | 10-15% |
| Fossiliferous deposit | *2-10% | | 15-20% | *50% | | 1% | | - | 10% | - | 2-10% |
| Phosphatic deposit | *10-15% | | 35% | *10% | | *2-3% | | - | 20-30% | 3-5% | 2-5% |
| Silty-Shaly (wavy) Interlaminated deposit | *20% | | 25% | *30% | | *15% | | - | - | 8-10% | - |
| Dolomitic mudstone | *10% | | 20-30% | *2-20% | | 30-40% | 40-80% | - | - | - | - |
| Micritic/Limy Mudstone | *10% | | 40% | *30-40% | | *5% | | - | - | - | 5% |

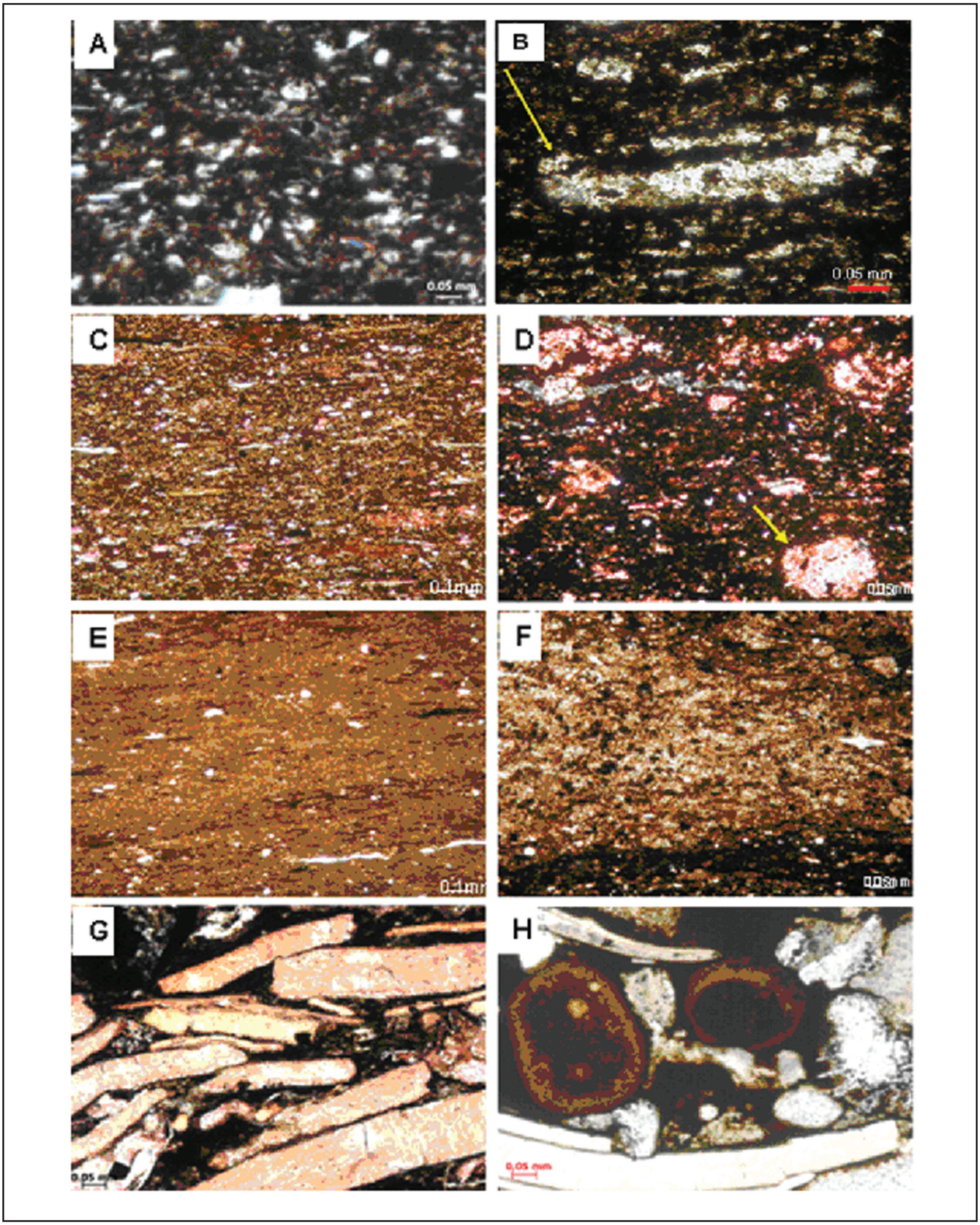


**Figure 2**. *Photomicrographs and core photograph of the nine lithofacies. A) shows the high amount of detrital quartz often found in Siliceous Non-calcareous Mudstone, B) Agglutinated forams in Siliceous Non-calcareous Mudstone, C) Relative abundance of calcite (pink color stained grains) in Siliceous Calcareous Mudstone, D) Calcite (pink stained grains) filling the probable burrows (yellow arrow) in Siliceous Calcareous mudstone, E) Micritic/Limy Mudstone, F) Reworked spicules in Bottom current calcareous laminae deposit, G) Fossiliferous deposit showing macrofossil shell fragments, H) Surficially coated phosphatic ooids in fossiliferous deposit, I) Silty-shaly (wavy) inter-*

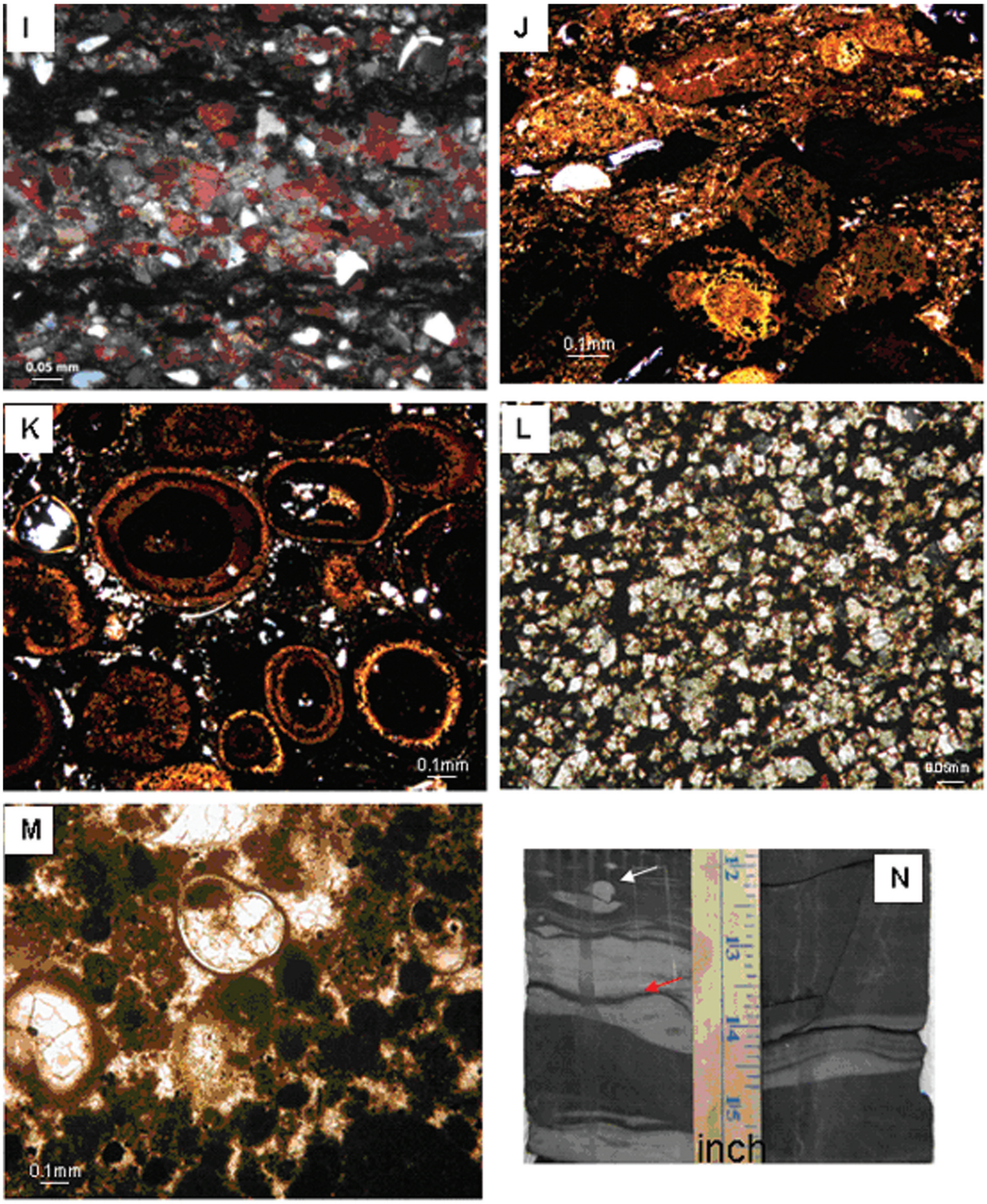


**Figure 2** - *continued*

*laminated deposits: abundant silt size quartz and calcite grain (pink stained grains) interlaminated with clay, J) Phosphatic fecal pellets, K) Well developed phosphatic ooids, L) Dolomitic mudstone, M) Well preserved microgastropods and pelloids in concretion, N) Core photo of Bottom current calcareous laminae deposit: white arrow shows Teichichnus trace fossil, red arrows shows the current lamination and ripple structures.*

***Siliceous Calcareous Mudstone***

The *siliceous calcareous mudstone facies* is black, massive mudstone which effervescences with dilute hydrochloric acid. The calcareous mudstone facies has a composition very close to that of the siliceous, non-calcareous mudstone, except that calcite constitutes from 5% to 40% of the total composition (Table 1). The calcite occurs as sparry calcite fillings in probable burrows (Figure 2D), or as tiny broken skeletal fragments.

***Micritic/Limy Mudstone:***

The *micritic/limy mudstone facies* is composed of autocthonous calcite mud (Figure 2E) with low abundance of microfossils and small amounts of scattered invertebrate fauna, shell fragments and detrital silt size grains (Table 1). This facies represents a change of depositional environment to relatively shallow water conditions. The widespread micrite forming the matrix suggests that the depositing water was relatively warm to provide autochthonous and skeletal calcite sediments. The horizontal lamination and lack of significant bioturbation suggests that the lime was being deposited in a quiet water setting, though shallower than the preceeding two muddy facies.

***Bottom Current Calcareous Laminae Deposit:***

This facies is represented as calcite rich laminae, which are horizontal and parallel to bedding. Very often they exhibit sedimentary structures such as ripples and cross lamination (Figure 2N), suggesting bottom current activity. Often, such fine-grained sediments can become subjected to reworking by bottom currents (Figure 2F) which are expressions of oceanic thermohaline circulation (Stow et al. 1996, Stow et al. 2001,). These features are also affected by diagenesis in the form of secondary lensoid growth of the calcite rich laminae. This facies is invariably bioturbated and contains forms including *Chondrites, Teichichnus, Phycosiphon, Cosmoraphe, Asterosoma and Planolites* indicating low oxygenation. Possibly the short-lived, oxygenation prevalent during deposition of this facies was conducive for organisms to dwell only for a short time and to be restricted only within this facies. Petrography reveals a high amount of calcite, pyrite, marcasite, minor quartz and clay minerals (Table 1).

***Reworked Fossiliferous Deposit:***

The *fossiliferous deposit* refers to thin laminae of broken macrofossil shell fragments, often in coalesced forms. The broken shell fragments, which include brachiopods, pelecypods and echinoderms, are very often accompanied with surficially coated phosphatic grains/ooids (Figure 2H) and intraclasts. This lithofacies is thought to have been deposited under relatively high energy conditions. Calcite is the dominant mineral (Table 1).

***Silty-Shaly (Wavy) Interlaminated Deposit:***

The *silty-shaly (wavy) interlaminated deposit* is not a common facies of the Barnett Shale, and occurs only in the Upper Barnett. Internally, this facies consists of alternate laminae of silt and mud (Figure 2I). The silts are composed of detrital quartz, calcite and glauconite grains. The average grain size is 0.05mm. Very often there are several broken shell fragments and a few arenaceous, agglutinated forams. The relatively larger burrows associated with this facies, along with the subrounded to angular nature of the detrital grains, suggests a close proximity to a source/marginal basin setting and relatively shallow water conditions.

***Phosphatic Deposit:***

The *phosphatic* intervals range from < 1.25 cm to 3.75cm in thickness and mostly consist of different forms, including pellets and ooids. The phosphatic pellets are subrounded to elongate in shape (Figure 2J). Often the pellets incorporate terrigenous grains of quartz and mica flakes, as well as microfossils. Wignall (1994) suggested that phosphatic fecal pellets are good agents for removal of both terrigenous and biogenic material through the water column. He noted that they are commonly preserved in low energy environments. A rare, but magnificent record of good concentric cortex ooid forms of the phosphatic deposit occur in the Barnett Shale (Figure 2K) which suggests winnowing in an energetic marine environment. Poorly developed forms with surficial concentric rings are more common.

***Dolomitic Mudstone:***

*Dolomitic mudstone* is composed mostly of rhombohedral dolomite crystals (Figure 2L). They commonly contain a high amount of calcite shell fragments which suggests secondary, diagenetic dolomitization of initially fossiliferous mudstone. Sometimes dolomite rhombohedral grains are embedded in clayey matrix. The origin of the dolomitic mudstone is thought to be secondary, diagenetic alteration.

***Concretion:***

*Concretions* within the Barnett Shale are calcareous in nature. They range from <5 cm to .45 m in thickness. They are found in equal abundance in both the Upper and Lower Barnett. Concretions are common diagenetic products and generally are thought to be syngenetic (early diagenetic) as well as epigenetic (late diagenetic) in origin. Carbonate concretions are common in shales (Weeks, 1953). When developed in their early stages when the enveloping mud was still unlithified, the concretions tend to preserve full bodied, uncompressed microfossils (Figure 2M) within them and the enveloping shales are bent and compacted around the nodular form. However, when developed in later stages (epigenetic), concretions generally exhibit continuous bedding through them.

## Well Log Characteristics of Lithofacies

Some lithofacies have very distinctive log signatures (fig. 3). Phosphatic deposits exhibit a characteristic high gamma ray value, due to a high amount of Uranium (detected on a spectral gamma ray log). The association of Uranium with phosphates is common to many other marine shales (Kochenov and Baturin, 2002). If sufficiently thick, calcite- rich fossiliferous deposits often affect the log response. The richness of transported phosphatic grains within fossiliferous deposits either increases or decreases the gamma ray response. A sharp contact between a less calcitic facies, such as siliceous calcareous mudstone, and more calcitic facies, such as micritic/limy mudstone, is represented by an abrupt decrease in the log response. Careful identification of the corresponding core-log response is imperative for identification of regional trends of vertical and lateral facies change and correlations in uncored wells.

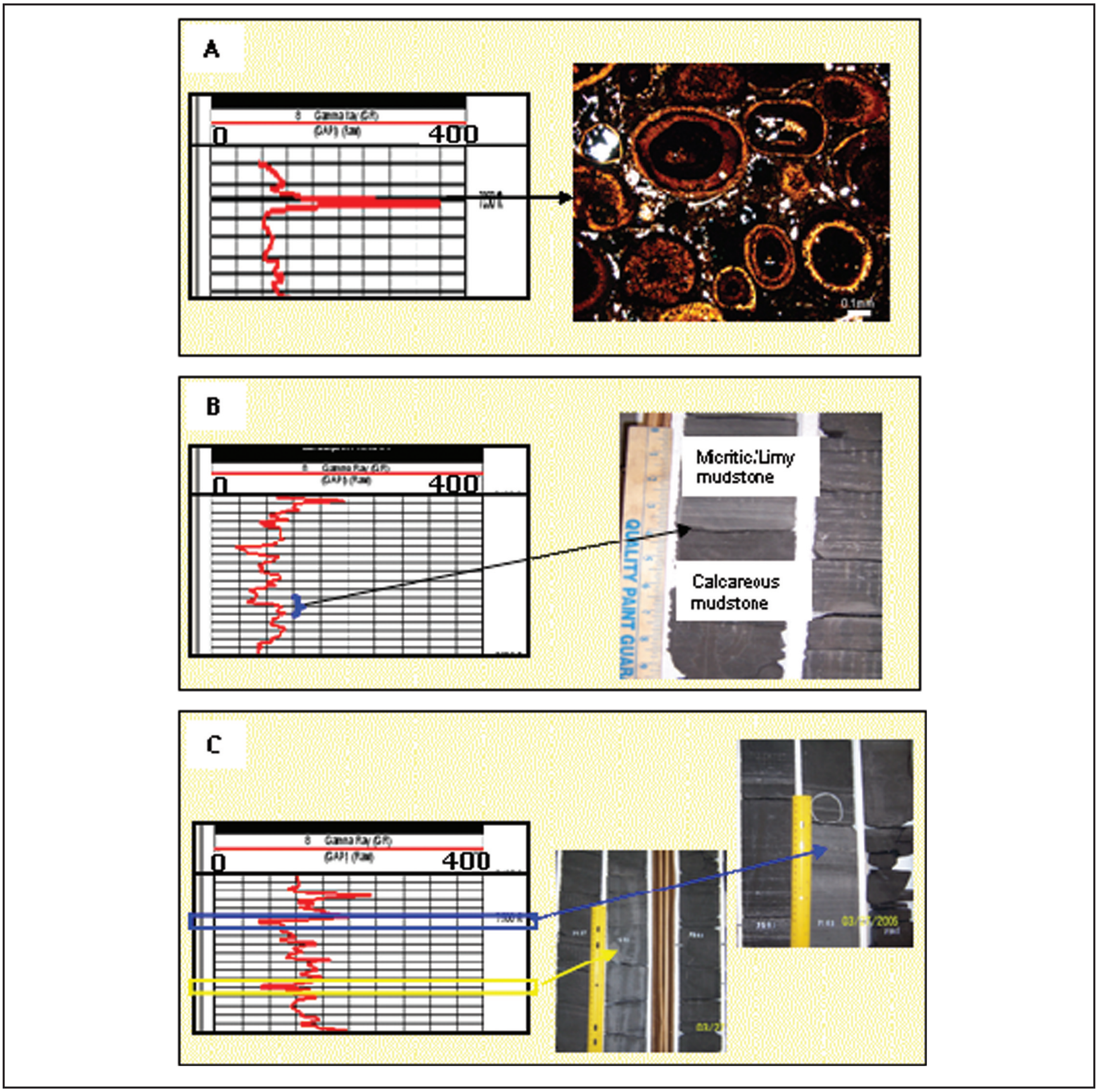


**Figure 3**. *Log responses of some lithofacies. A) Phosphatic ooid giving rise to remarkably high Gamma Ray response, B) Abrupt change in Gamma Ray values owing to sharp contact between Siliceous calcareous mudstone and Micritic/limy mudstone and C) Dolomitic mudstone ans reworked shelly deposits giving rise to low Gamma Ray values.*

**Log Stacking Patterns: High Resolution Depositional Parasequences**

The gamma ray profile has been successively used in the past for regional correlation in several shale formations (Schieber, 1998). For this study, cyclic stratal stacking patterns were identified from the gamma ray profile i.e. upward-increasing intervals, upward-decreasing intervals and intervals of constant API. The log pattern and the stratal characteristics suggest that these increasing and decreasing gamma ray intervals represent high resolution parasequences, defined as relatively conformable successions of genetically related beds or bedsets bounded by marine-flooding surfaces (Van Wagoner et al. 1990). Figure 4A shows two upward 'cleaning' parasequences. In clastic strata, this pattern is indicative of upward increase in grain size and usually in quartz content. In the Barnett Shale, the pattern is a result of upward change in mineral composition, as described below.

These log parasequences were analyzed in detail in the core to identify the factors attributing to the systematic, cyclical gamma ray patterns. One of the upward-decreasing gamma ray parasequences is detailed here in Figures 5 and 6.

Petrographic analyses of the upward-decreasing gamma ray parasequence (Fig. 5) from 7596.5′ to 7622.5′ in well B show that the basal part of the parasequence is characterized by *phosphatic shales* and siliceous microfauna (Fig. 4(1)). Moving upsection, there is a relative increase in detrital calcite grains, and detrital silt and loss of biosiliceous component (Fig. 4(2)). The top of this particular parasequence consists of *dolomitic mudstone* composed of dolomite rhombs mixed with scattered broken fragments of macrofossils (Fig. 4(3)). This interval is probably an altered product of a once-fossiliferous mudstone. The upward increase in carbonate content and decrease in total clay is suggestive of the change in the sediment sup-

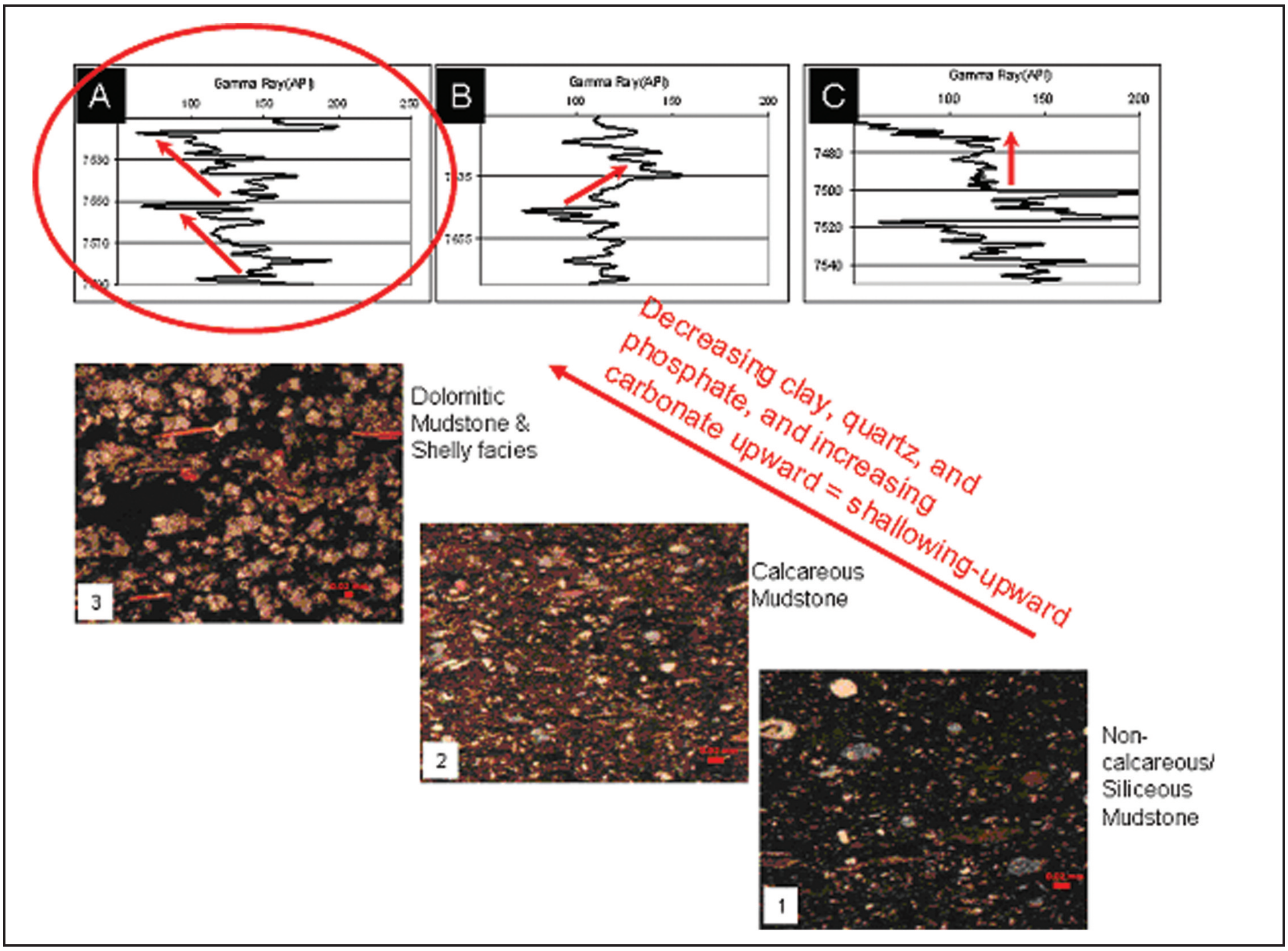


**Figure 4**. *Example of (A) upward- decreasing Gamma Ray-, (B) upward- increasing Gamma Ray-, and (C) Constant Gamma Ray- parasequence patterns of the Barnett Shale from cored well B. Photomicrographs of an upward-decreasing gamma-ray parasequence shown in Figure 5 are shown: 1) The base of the parasequence, at 7620.8′ contains quartz as biogenic spicules and as terrigenous silt, a high amount of phosphate pellets preserved as compacted, elongate lenses in the matrix, and ferroan dolomite stained blue. (2) Middle of this parasequence, at 7606.4′, is characterized by a high amount of detrital silt, pink -stained calcite detrital grains and relatively reduced amounts of clay matrix. (3) Top of the parasequence, at 7598.3′, consists of dolomitic mudstone wherein originally fossiliferous mudstone has been diagenetically altered. Relative high abundance of the broken macrofossil fragments is present in the matrix.*

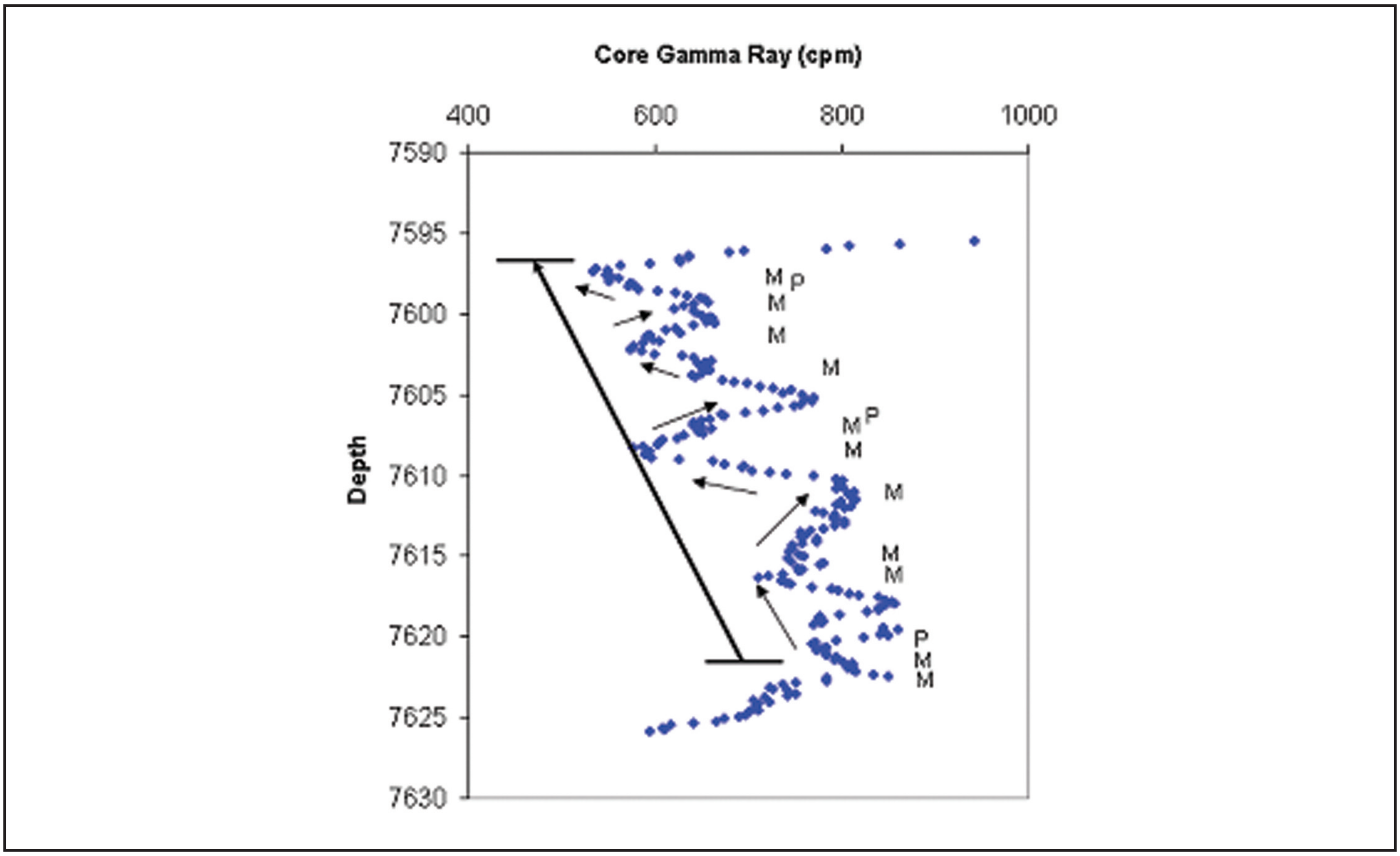


**Figure 5**. *Core Gamma Ray plot for the upward – decreasing Gamma Ray parasequence from well B. Depths at which mineralogical and petrographic analyses were conducted are marked as M and P, respectively. The arrows mark the two scales of parasequence.*

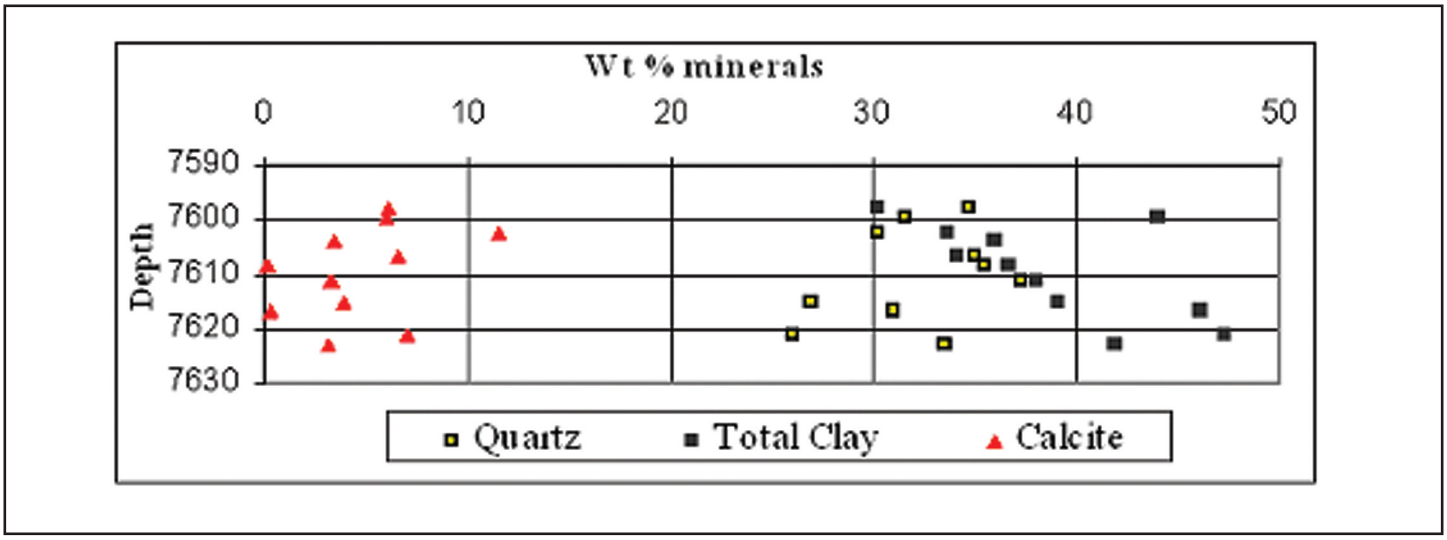


**Figure 6**. *Weight percentage of Quartz, Total Clay and Calcite content for the above upward-increasing Gamma Ray parasequence is shown. Mineralogic composition was determined by FTIR analysis.*

ply and environment. The relatively constant proportion of quartz could be explained by the fact that silica is being derived from two sources, providing an upward decrease of biosiliceous productivity or upward increase in terrigenous silt.

The two scales of cyclicity noted in Figure 5 are highly suggestive of eustatic sea level fluctuations which typically occur at different, superimposed geologic time scales. In this case, a parasequence set of five high-frequency parasequences is superimposed upon a single parasequence of longer duration. The absence of any age-datable fossils precludes determining the absolute time spans for these parasequences.

Similar work on core B has led to an interpretation of the parasequence stacking pattern in this well (Fig. 7). The interpretation is based on the position of significant surfaces such as erosional surfaces, sharp boundaries, and on vertical stacking patterns of relatively shallow water lithofacies (e.g. *Silty-shaly, wavy deposits* and *Micritic/limy mudstone*) with respect to deeper water lithofacies (e.g.

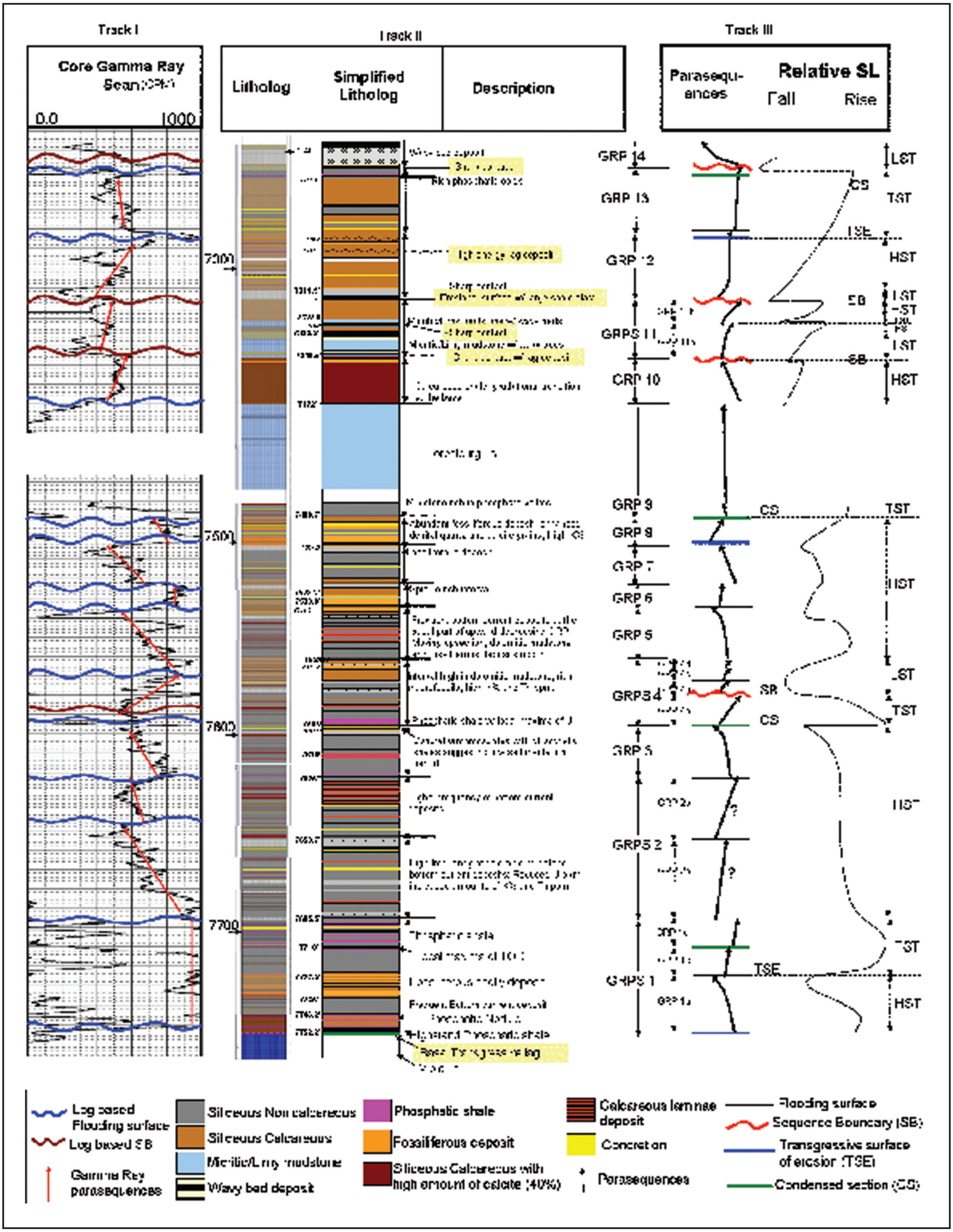


**Figure 7**. *Composite plot of well B depicting the core Gamma Ray parasequence, core description, core parasequence, interpreted relative sea level and positions of key stratal surfaces and systems tracts.*

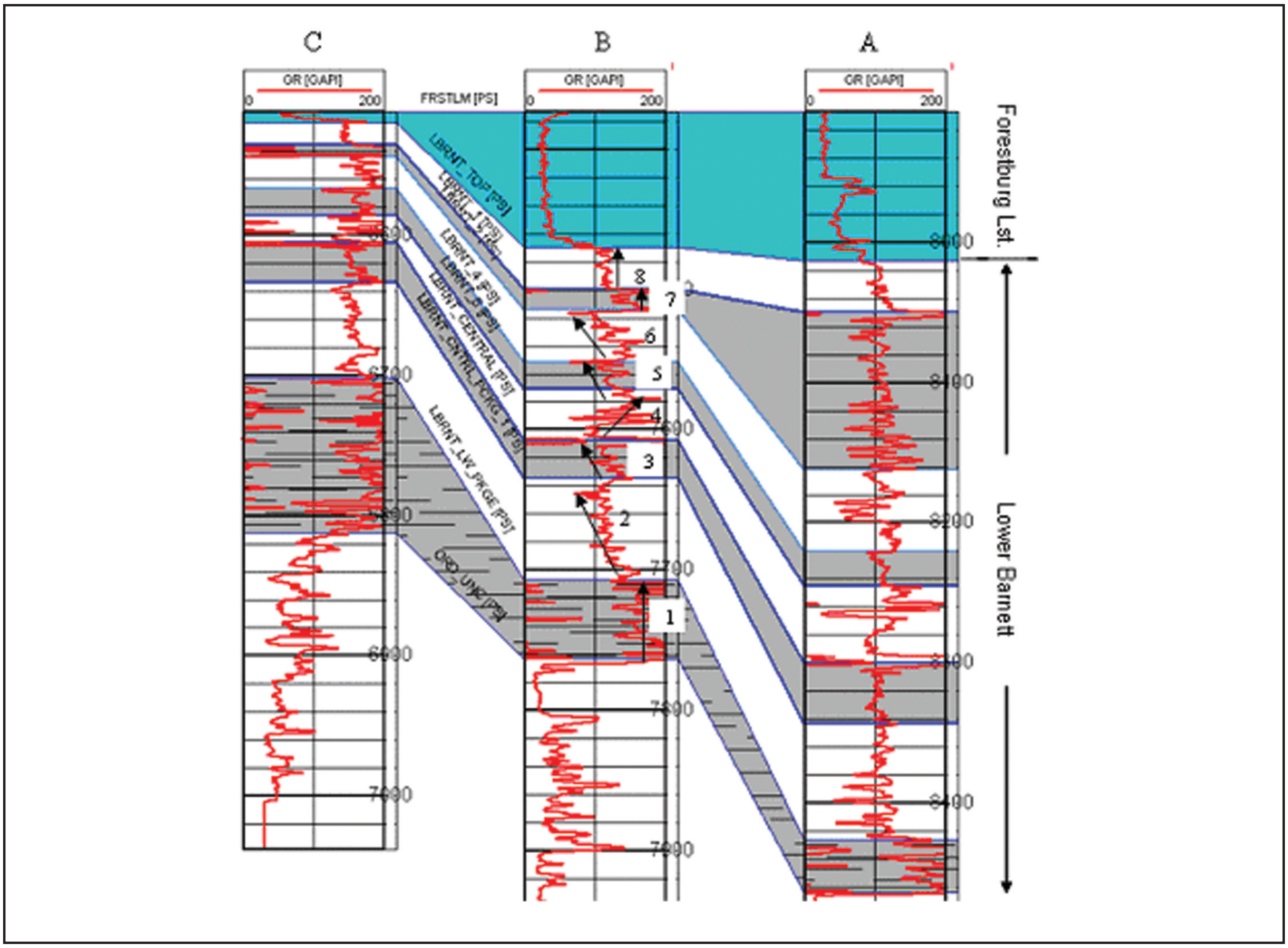


**Figure 8**. *Vertical stacking pattern and lateral correlation of the Lower Barnett parasequences in the cored wells. The stratigraphic datum used here is the top of the Forestburg Limestone. The eight Gamma Ray parasequence trends for the Lower Barnett are marked by arrows and numbered.*

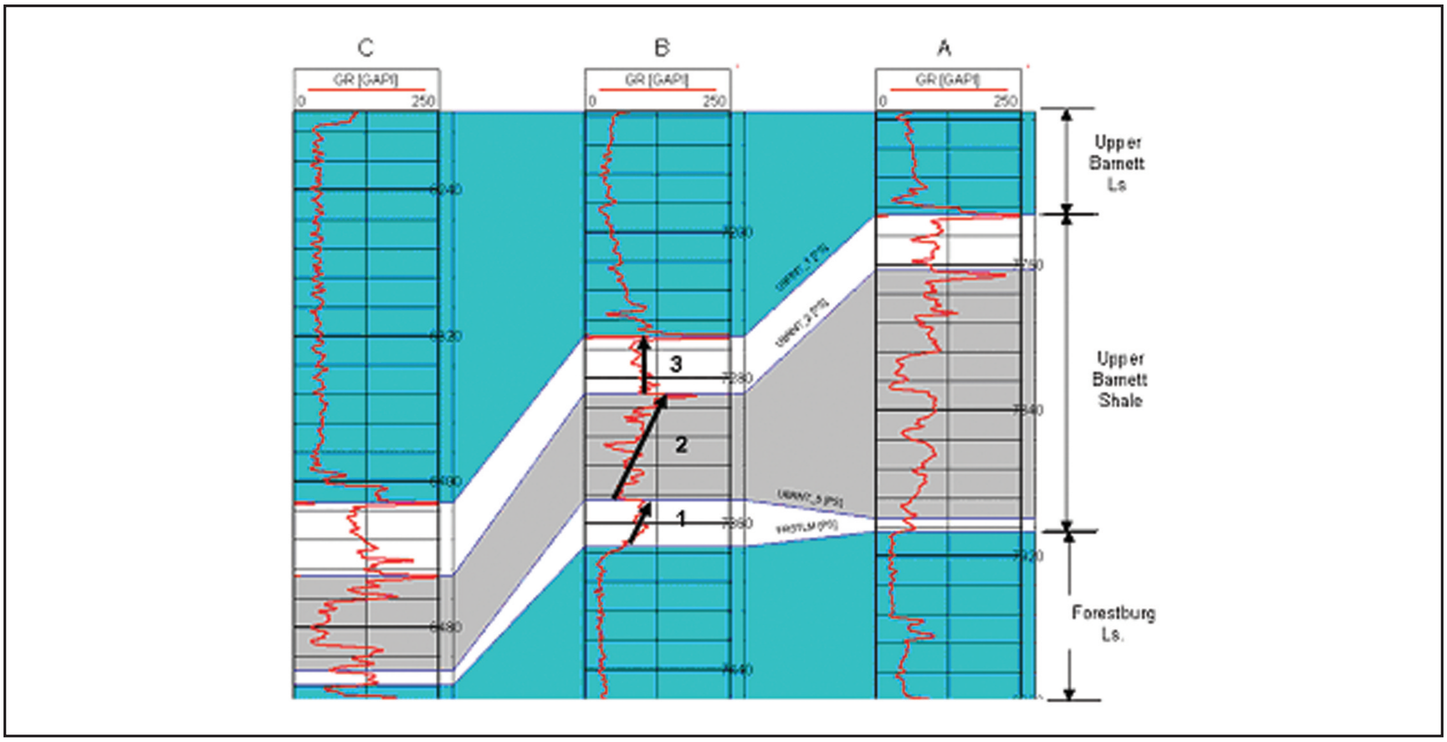


**Figure 9**. *Laterally correlatable parasequences of the Upper Barnett Shale in the cored wells. The datum is the top of Upper Barnett Limestone.*

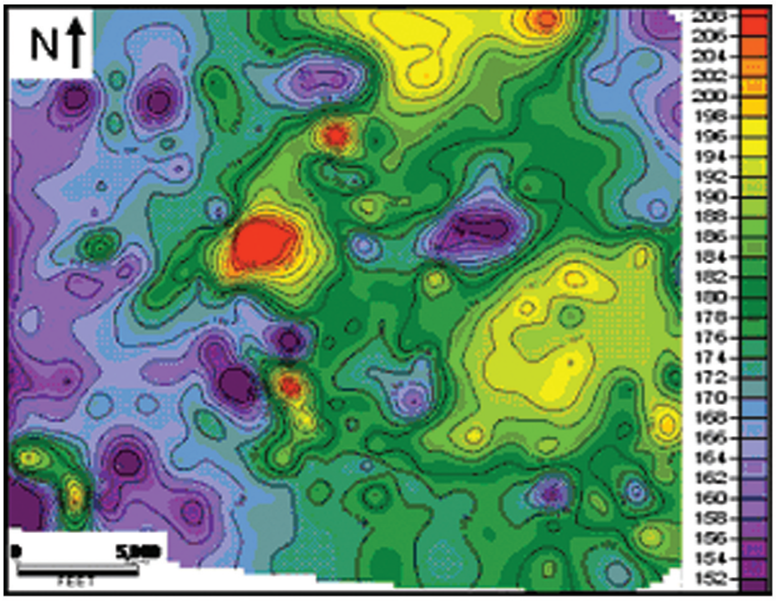


**Figure 10**. *Isopach map of combined parasequences #1, 2 and 3 of Lower Barnett Shale (Fig 8). Note the irregularities in the thickness pattern. (After Borges, 2007)*.

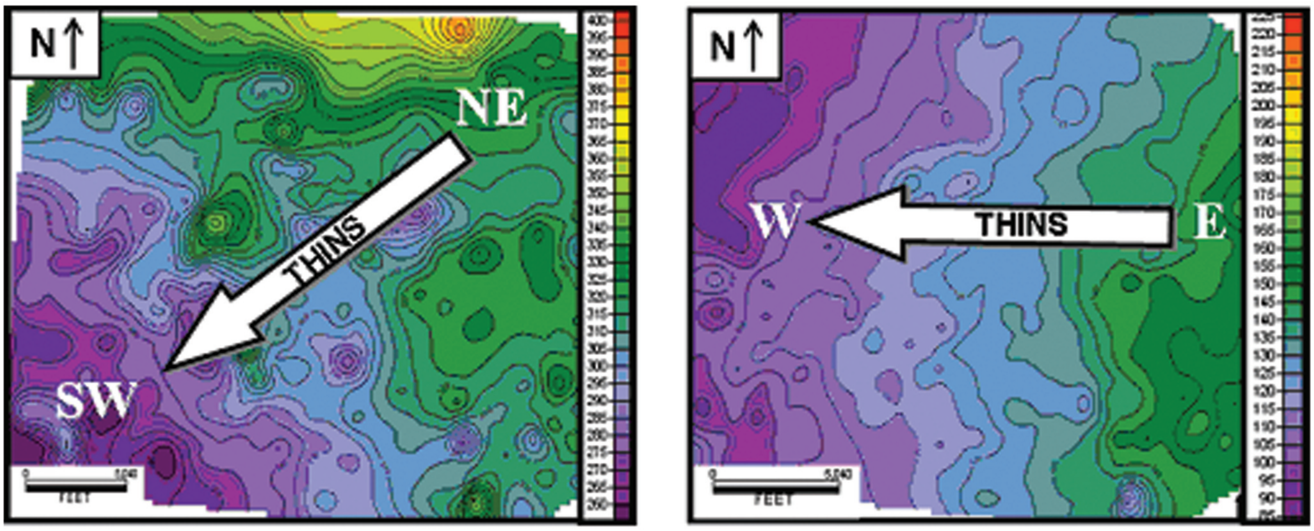


**Figure 11**. *Thickness map of the Lower Barnett Shale and Upper Barnett Shale for the seismic survey area #3 showing southwest to northeast trend and west to east trends, respectively. (After Borges, 2007)*

phosphatic shales) integrated with core gamma ray parasequences.

Such significant erosional surfaces are present in the Upper Barnett, suggesting a record of stratigraphic interruption in deposition and/or change in depositional energy conditions. Based on these surfaces, three possible sequence boundaries are documented for the Upper Barnett (Fig. 7). Although these surfaces were common in the Upper Barnett of well B, they are absent in the Lower Barnett. This is suggestive of a relatively deeper, quieter water setting during deposition of the Lower Barnett Shale. The Lower Barnett parasequences are best identified by the vertical stacking pattern of low energy phosphatic shales followed upward by high energy eroded, reworked fossiliferous deposits formed in response to a lowering of relative sea level. (Fig. 7).

The parasequences described above are laterally continuous, correlative and mappable (Fig. 8 and 9). Isopach maps were generated for these parasequences in seismic survey area # 1 (Fig. 1) using the 217 available wells, including cored well B (Borges, 2007). The isopach maps reveal variations in thickness trends among the Upper and Lower Barnett Shale parasequences. Interestingly, the peculiar, irregular isopach pattern of the combined basal three parasequences (Fig. 10) is thought to depict the paleotopography of underlying karst collapse features at the top of the Viola Limestone (Borges, 2007). The entire Lower Barnett Shale thickens toward the northeast (Fig. 11), while the Upper Barnett Shale thickens toward the east.

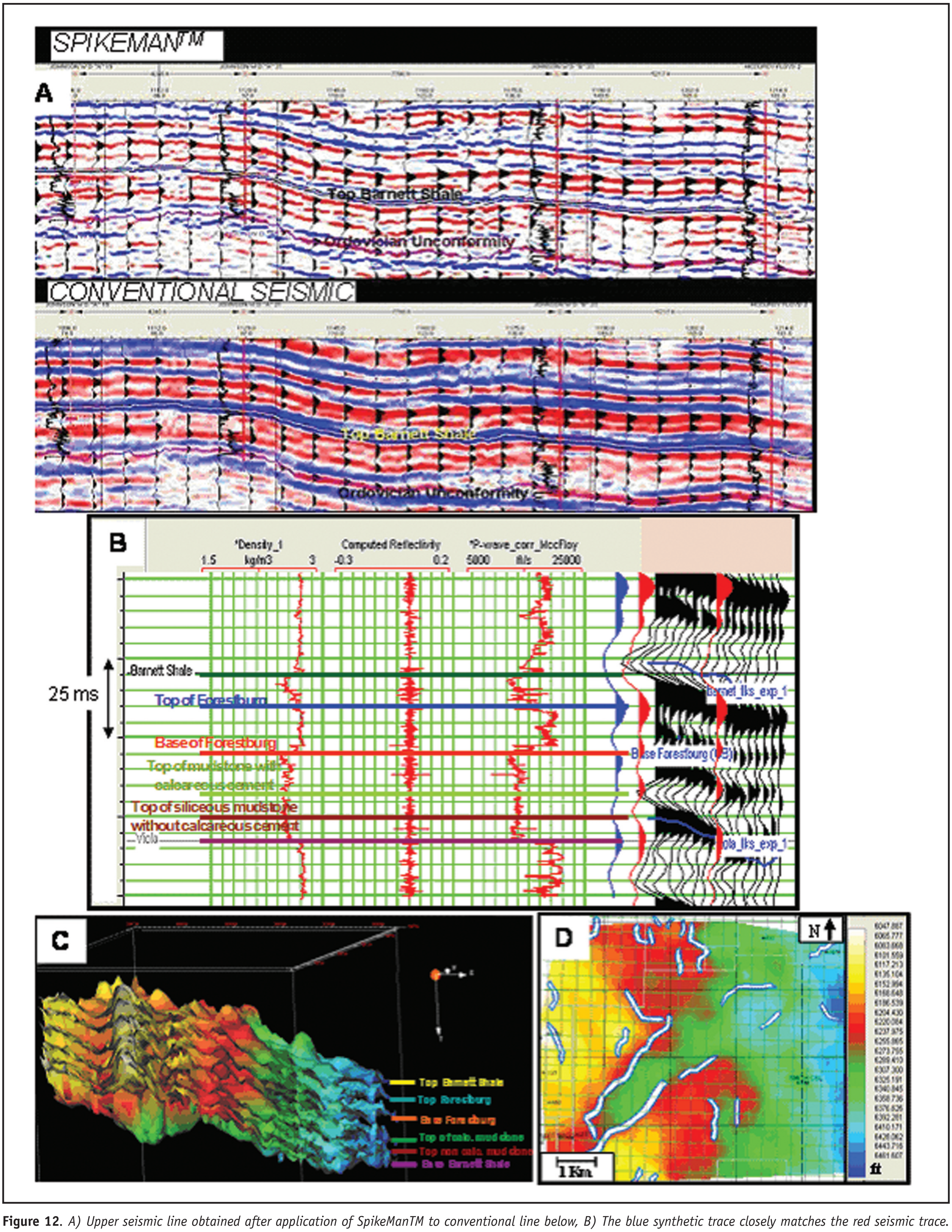


**Figure 12**. *A) Upper seismic line obtained after application of SpikeManTM to conventional line below, B) The blue synthetic trace closely matches the red seismic trace. The five intervals corresponding to the reflections on seismic and synthetic traces were correlated to lithofacies, C) 3D view of the five interpreted horizons and D) Interpreted Structural map of the top of the Barnett Shale of Survey area #1 (After Borges, 2007). Hot colors are shallower and cool colors are deeper.*

## Seismic Stratigraphic Analysis

Three 3D seismic volumes (Fig.1) have been related to well log and core characterizations. Seismic survey #1, located in the center of Newark East field, consists of 240 inlines and 200 crosslines spaced about 33.5 m apart. The cored well B was used to calibrate stratigraphy to the seismic.

Conventional 3D seismic volumes display high amplitude reflectors between the top and base of the Barnett Shale, indicating the presence of seismically resolvable internal stratigraphy (Borges, 2007). Special processing was applied to the conventional seismic data to improve definition of high resolution events (Fig. 12A). The reflections on the seismic and synthetic trace were related to lithological changes defined by core description and calibrated to the well logs (Fig. 12B). The reflections represent boundaries between five lithologic intervals – Top Upper Barnett Shale, Top Forestburg Limestone, Top Lower Barnett Shale, and tops of two recognizable intervals within the Lower Barnett Shale. These intervals were mapped throughout the seismic survey area (Figure 12C). The various depth structure maps obtained by application of an average velocity map shows a common west to east deepening trend with twenty five identifiable faults (Fig. 12D). The trends of interval thickening are variable within the Barnett Shale (Fig. 13) which is suggestive of changes in the depositional setting and/or the geometry of the basin during deposition of the Barnett Shale.

Seismic survey area #2 is located in the south center of the Newark East field, to the south of seismic area #1 (Fig. 1). This survey was merged with the survey from area #1 in order to regionally expand a seismic stratigraphic interpretation and further document the general structural setting and thickening trends. This merged area consists of 480 Inlines and Crosslines with an increment of 1 and a spacing of 33.5 m. Synthetic traces were created from well logs in order to tie the geology to the merged seismic volume. Seismic interpretation of the 3D survey led to delineating and mapping of six horizons (top of Upper Barnett Shale, top of Forestburg limestone, top of Lower Barnett Shale, two mappable horizons within Lower Barnett Shale and top of Viola limestone) (Figure 14A). Figure 14B, C and D shows the time structure map for these horizons. The seismic maps reveal a deepening

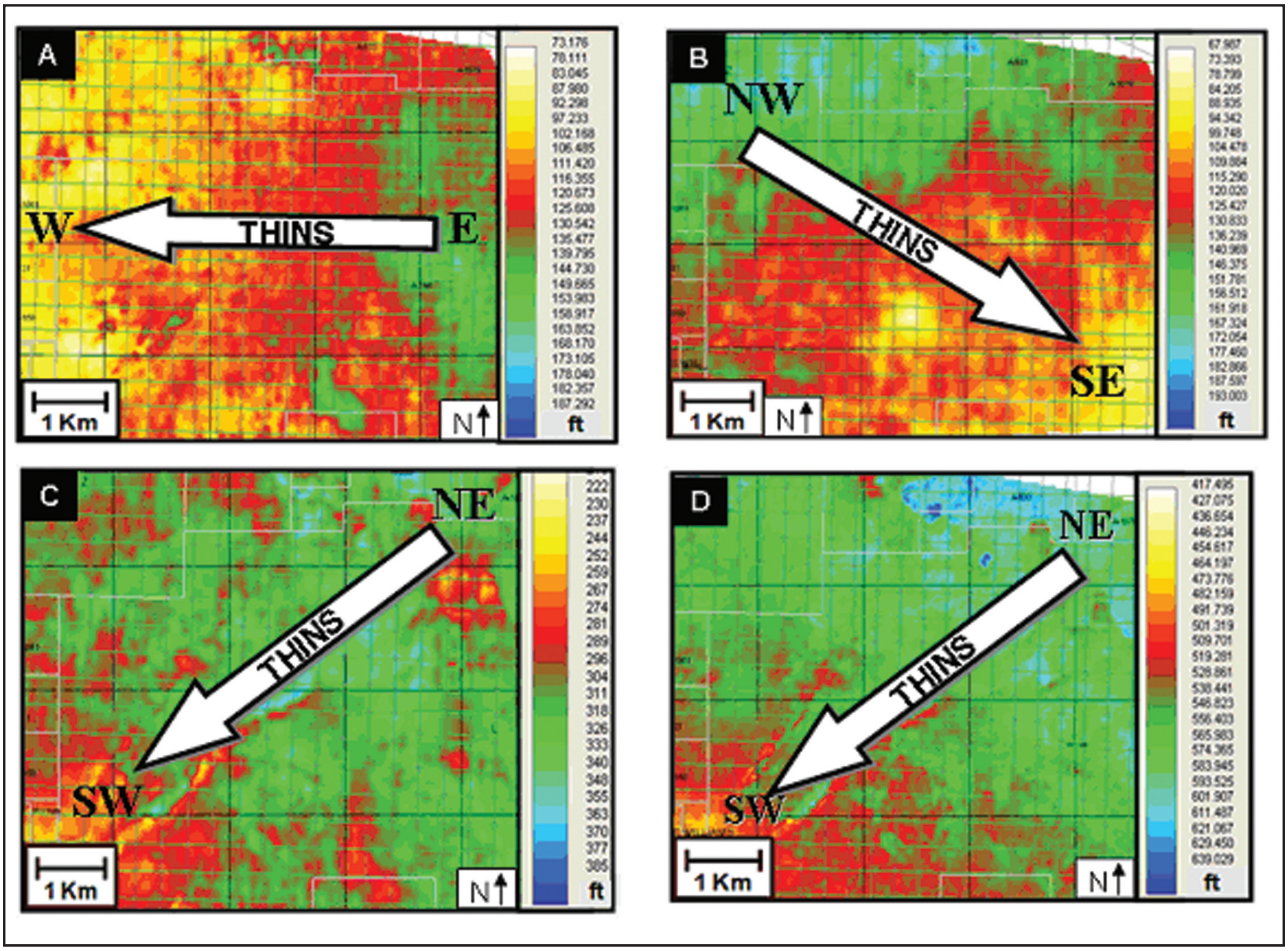


**Figure 13**. *The isopach maps and trends of thickness for: (A) Upper Barnett Shale, (B) Forestburg Limestone, (C) Lower Barnett Shale and (D) Entire Barnett interval. Hot colors are thinner and cool colors are thicker.*

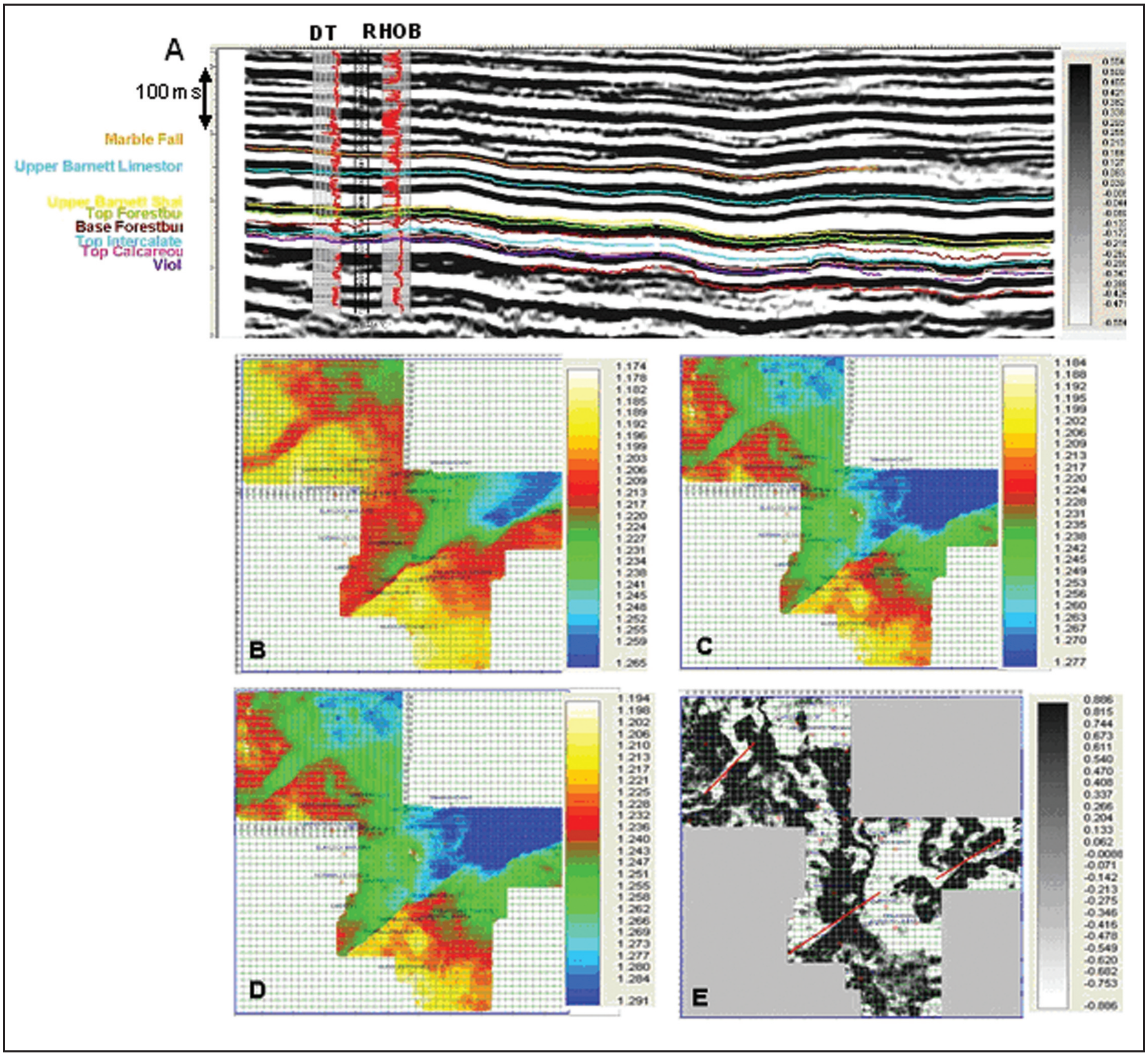


**Figure 14**. *A) Seismic line through the merged survey area (Seismic area #1 and 2) showing the interpreted tops, B) Structure map of top of Upper Barnett Shale, C) Structure map of top of Forestburg limestone, D) Structure map of top of Lower Barnett Shale and E) Time slice showing coherency of the merged survey. Red solid lines mark the location of possible major faults. Color code for figures B, C, and D are the same as used in Figure 12 D.*

trend toward the northeast for the entire Barnett Shale, which is consistent with the literature (Montgomery et al 2005, Pollastro et al. 2007). A coherency cube created for the merged survey, helped identify faults in the area (Figure 14E).

Survey Area #3 is located in the eastern part of the Newark East field and does not contain any cored wells (Fig. 1). Thus, this seismic volume was studied independently in order to illuminate the information provided by seismic data with uncored wells. The seismic survey area consists of 200 Inlines and Crosslines with an increment of 1 and a spacing of 91 m. This survey was recorded with a sample interval of 0.002 and has 2001 samples per trace. The survey area contains seven wells whose density (RHOB) and sonic (DT) logs were used to identify the tops of the Upper Barnett Shale, Forestburg, Lower Barnett Shale and Viola limestone. The matching reflectors were identified in the seismic volume and, hence, several isopach maps were generated for the stratigraphic intervals using the velocity values from each velocity log (Fig. 15). Within the Lower Barnett interval, some subtle, continuous internal reflections are present (Fig. 15A). However, the top and base of these reflectors are below the resolvable limit of the seismic. To improve the vertical resolution, model-based inversion was applied to the prestack seismic, thus allowing estimation of P- and S-impedances and density; neural net analysis was then applied to determine the relationship between the two

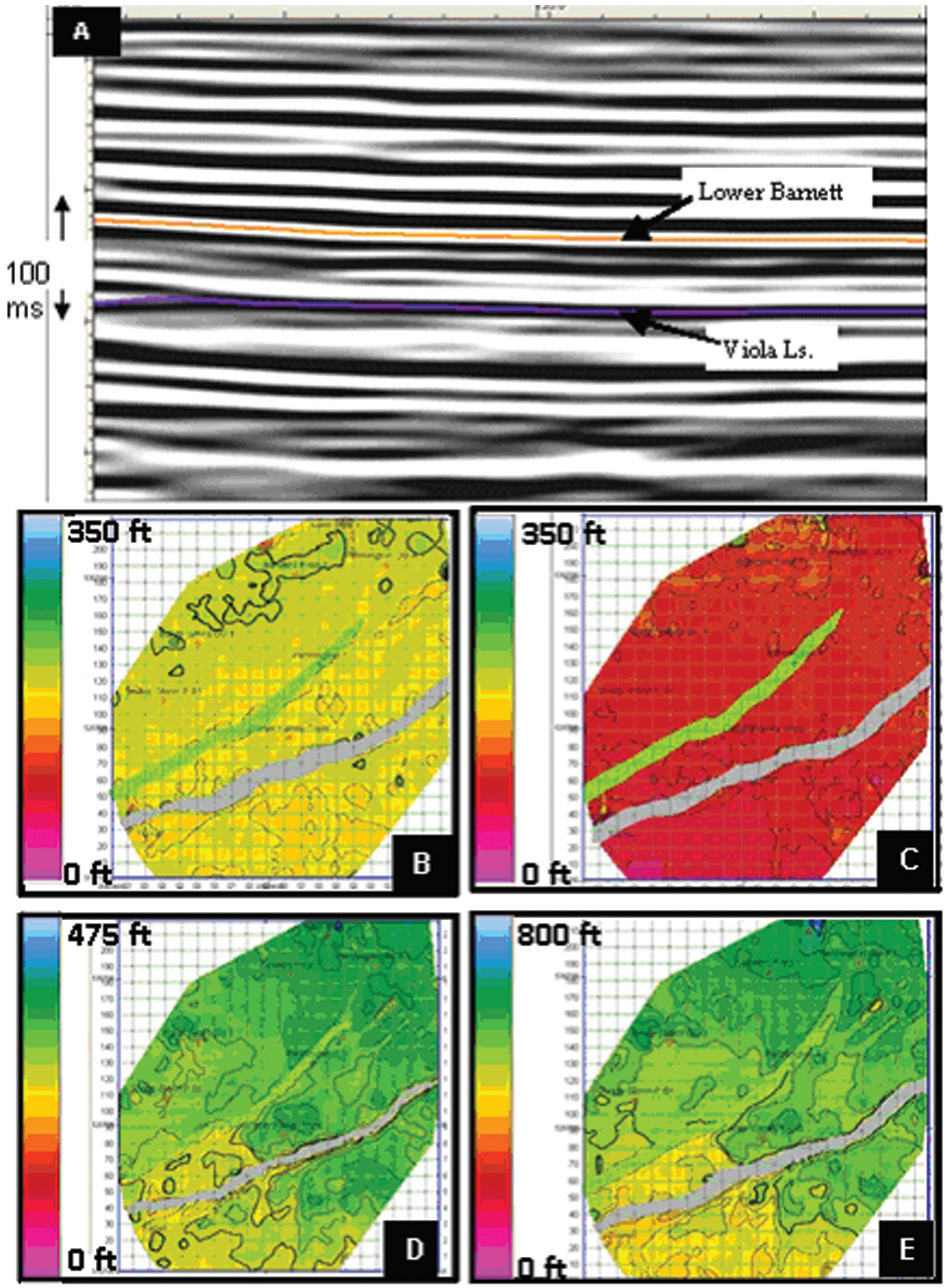


**Figure 15**. *An arbitrary line from Seismic survey area #3. Isopach Maps of B) Upper Barnett Shale, C) Forestburg limestone, D) Lower Barnett Shale and E) Entire Barnett Shale*

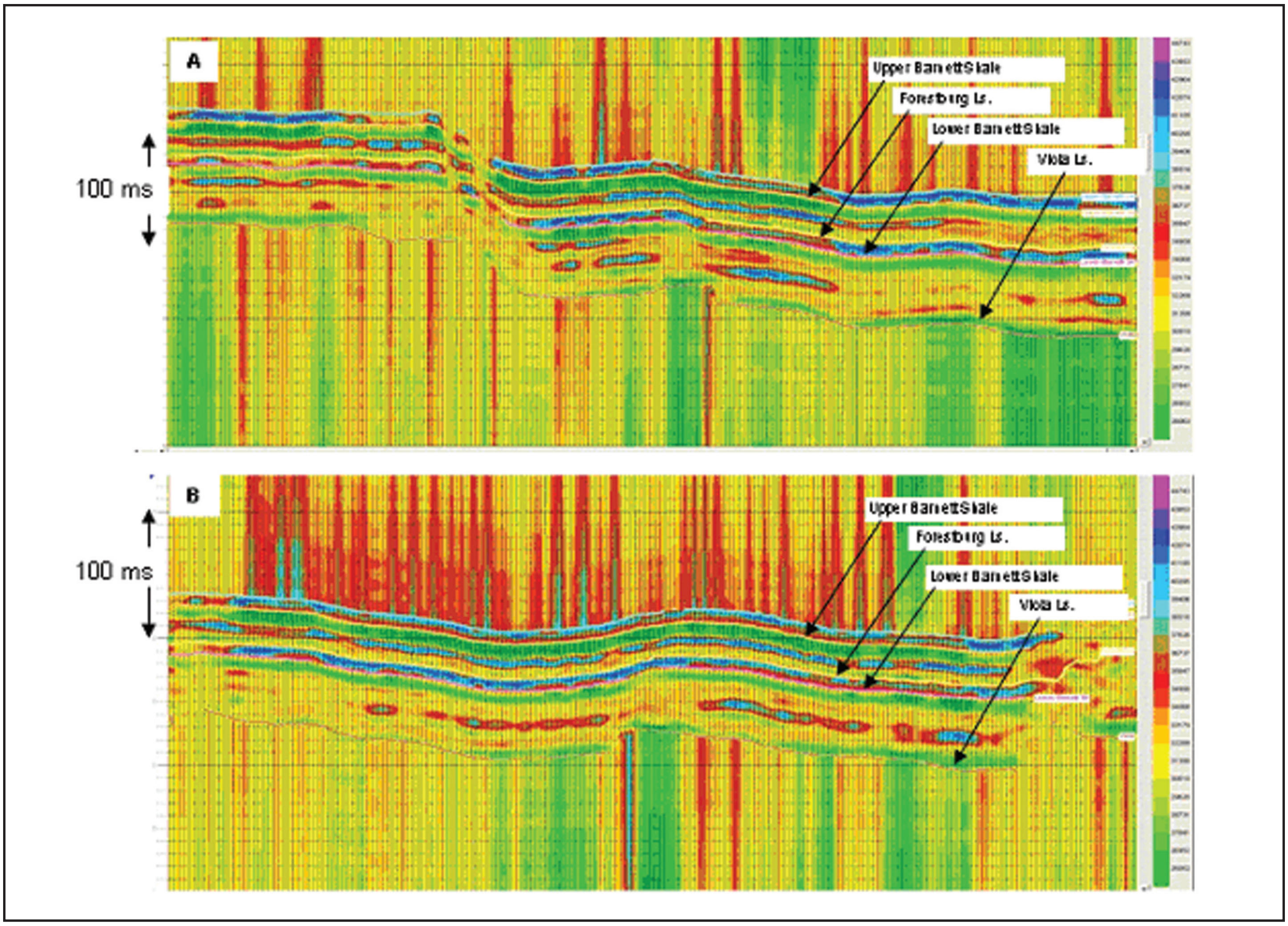


**Figure 16**. *Examples of (A) Inline and (B) Crossline sections showing the enhanced internal geometry of Lower Barnett after application of Neural network.*

types of data sets (i.e. well log and seismic data) for application to the entire 3D seismic volume. Fig. 16 shows that the resolution of the four intervals within the Lower Barnett Shale has been improved, revealing substantial variability in the Lower Barnett.

## CONCLUSIONS

1) Detailed core analysis has led to the identification of nine lithofacies within the Barnett Shale within the study area.

2) Parasequences have been defined on the basis of gamma ray log response coupled with lithofacies identification. Carbonate-rich intervals are indicative of shallower water environments, and clay-rich intervals are more indicative of deeper water, less energetic environments of deposition. These parasequences are continuous and mappable across the study area. Parasequences reveal a systematic vertical stacking pattern with these and related lithofacies.

3) Three 3D seismic surveys in the area reveal internal stratigraphy of continuous and mappable, reflectors using enhanced techniques. The internal stratigraphy is correlative with stratigraphic intervals defined by well logs and core. Seismic interval mapping shows a thickening trend of the Barnett Shale toward the northeast.

4) Integrated analysis of Barnett Shale logs, core and seismic has provided additional insights into its variability, and provides a means of regional mapping of stratigraphic intervals.

**REFERENCES CITED**

(The Oklahoma City Geological Society (OCGS), and the Shale Shaker Editorial Board, are not responsible for omissions of references cited in the text.)

Adams, J.E., 1954, Mid-Paleozoic Paleogeography of Central Texas: Shale Shaker v.4, no.6, p. 4-9.

Borges, G., 2007, Seismic Sequence Stratigraphic Interpretation of Barnett Shale at Newark East Field in Fort Worth Basin, Texas: Unpublished Master's thesis, University of Oklahoma, Norman, Oklahoma, 72 p.

Durham, L.S., 2007, Barnett 'Hits' don't rule out misses still a 'statistical' play: AAPG Explorer, October 2007.

Henry, J. D., 1982, Stratigraphy of the Barnett Shale (Mississippian) and associated reefs in the northern Fort Worth basin: Dallas Geological Society paper, 21 p.

Kochenov, A.V. and G. N. Baturin, 2002, The paragenesis of organic matter, Phosphorous and Uranium in Marine sediments: Lithology and Mineral Res. v. 37, no. 2, p. 107-120

Milliken, K., S. Choh, P. Papazis, and J. Schieber, 2007, 'Cherty' stringers in the Barnett Shale are agglutinated foraminifera: Sedimentary Geology. 198, p. 221-232.

Montgomery, S.L., D.M. Jarvie, K.A. Bowker, and R.M. Pollastro, 2005, Mississippian Barnett Shale, Fort Worth basin, north-central Texas: Gas-shale play with multi-trillion cubic foot potential: AAPG Bulletin, v. 89, no. 2, p. 155-175.

Papazis, P.K., 2005, Petrographic characterization of the Barnett Shale, Fort Worth Basin, Texas, Master's Thesis, University of Texas at Austin, Austin, Texas, 142 p.

Schieber, J., 1998, Developing a sequence stratigraphic framework for the Late Devonian Chattanooga Shale of the southeastern US: relevance for the Bakken Shale, in J.E. Christopher, C.F. Gilboy, D.F. Paterson, S.L. Bend, eds., Eight International Williston Basin Symposium, Saskatchewan Geological Society, Special Publication No. 13, p. 58–68.

Stow, D.A.V., A. –Y. Huc, and P. Bertrand, 2001, Depositional processeses of black shales in deep water: Marine and Petroleum Geology, v. 17, no. 4 p. 491-498.

Stow, D.A.V., H.G. Reading, and J.D. Collinson, 1996, Deep seas, in H.G. Reading, eds., Sedimentary environments: processes, facies and stratigraphy, Blackwell Scientific, Oxford, p. 395–454

Van Wagoner, J.C., R.M. Mitchum, K.M. Campion, and V.D. Rahmanian, 1990, Siliciclastic sequence stratigraphy in well logs, cores and outcrops: concepts for high resolution correlation of time and facies: AAPG Methods in Exploration Series, no.7, 53 p.

Weeks, L.G., 1953, Environment and mode of origin and facies relationships of carbonate concretions in shales: Journal of Sedimentary Petrology, v.23, no. 3, p. 162-173.

Wignall, P.B., 1994, Black Shales: Oxford Science Publication, 127 p.

Verish, N.P., 1979, Reservoir trends, depositional environments, and petroleum geology of "Cherokee" sandstones in T11-13N, R4-5E, Central Oklahoma: Shale Shaker, v. 29, nos. 9 & 10, pp. 209; 224-237.

Zeliff, C.W., 1976, Subsurface analysis, "Cherokee" Group (Pennsylvanian), northern Kingfisher County, Oklahoma: Shale Shaker, v. 27, nos. 1, 2, & 3, pp. 4-6; 24- 32; 44-56.